Chemical Physics Letters 709 (2018) 116–124

Contents lists available at ScienceDirect

Chemical Physics Letters

journal homepage: www.elsevier.com/locate/cplett

Research paper

Modeling selective ion adsorption into cylindrical nanopores

Yu Qiao[a,b], Cheng Lian[a,c], Benzhuo Lu[b,*], Jianzhong Wu[a,*]

[a] Department of Chemical and Environmental Engineering, University of California, Riverside, CA 92521, USA
[b] State Key Laboratory of Scientific and Engineering Computing, National Center for Mathematics and Interdisciplinary Sciences, Academy of Mathematics and Systems Science, Chinese Academy of Sciences, Beijing 100084, PR China
[c] State Key Laboratory of Chemical Engineering, East China University of Science and Technology, Shanghai 200237, PR China

HIGHLIGHTS

- Classical density functional theory is used to study ion selectivity.
- A neutral pore selects large ions, regardless of the pore size and ion composition.
- A large charged pore prefers adsorption of small counterions.
- A small charged pore selects large counterions.

ARTICLE INFO

Keywords:
Ion selectivity
Cylindrical pore
Density functional theory

ABSTRACT

Ion selectivity by cylindrical pores has been investigated using the primitive model of electrolytes and the classical density functional theory. It is found that a neutral pore always exhibits the preferential adsorption of large ions, regardless of the pore size and the bulk electrolyte composition. For a charged nanopore, however, the pore selectivity depends not only on the ion size but also on the pore radius as well as the surface electrical potential. While a nanopore prefers adsorption of small counterions when its radius is sufficiently large, it can be large-ion selective when its size becomes comparable to the ion diameters.

1. Introduction

Ion selectivity plays an important role in diverse electrochemical and biomolecular systems [1,2]. One outstanding example is the selective transport of ionic species through protein channels, which control a large number of physiological processes such as regulation of cytoplasmic calcium concentration and acidification of specific subcellular compartments [3]. Understanding ion transport under confinement is crucial to fulfill the great potential of nanofluidic devices as well as to design and optimize various porous electrodes for energy storage and conversion, new electrochemical devices for DNA sequencing, and nanofiltration membranes for novel separation and purification processes [4,5].

While the types of ion channels in living cells are numerous, a common feature is their unique capability to manipulate ion transport with high selectivity and passage rate. A wide range of molecular models have been proposed to unveil the thermodynamic behavior and kinetic mechanisms underlying the selective permeation of ions through different channels [6]. The theoretical investigations are mostly based on different forms of molecular dynamics (MD) [7], Monte Carlo (MC) simulations [8] and the classical density functional theory (DFT) [9]. The theoretical and simulation methods are complementary to each other. While MD/MC simulations are able to account for the atomic details of biomacromolecular systems, classical DFT studies are able to provide the essential physics of ion transport in nanopores by using simple coarse-grained models. In addition to drastically reducing the computational cost, the classical DFT is valuable to bridge the gap between experiment, simulation and the continuous equations of transport phenomena. For example, the fundamental measure theory (FMT) [10] is now commonly used to account for the ionic excluded volume effects neglected in the Poisson-Nerst-Planck (PNP) equation [11,12]. It has been shown that the modified PNP equation provides a more faithful description of ion stratification near a charged surface [13].

A number of previous investigations indicate that ion selectivity by a micropore is mainly determined by the relative size of ionic species, the pore radius, and electrostatic interactions [14–17]. The generic trends can be captured by relatively simple models of micropores and

* Corresponding author.
E-mail addresses: bzlu@lsec.cc.ac.cn (B. Lu), jwu@engr.ucr.edu (J. Wu).

https://doi.org/10.1016/j.cplett.2018.08.047
Received 5 June 2018; Accepted 17 August 2018
Available online 19 August 2018

ionic solutions. To mimic ion channels, the cylindrical pore model has been most widely used in both theoretical and simulation studies of ion selectivity. For example, Goulding et al. [14,15] used the classical DFT to investigate ion selectivity using a cylindrical pore of infinite length. They discovered that strong size selectivity is purely related to the pore size effects and that inclusion of electrostatic interactions shows no significant changes to the adsorption behavior. By investigating the distribution of uncharged particles in an infinite cylinder, Roth and Gillespie [16] found that a channel with strong surface attraction is always small-ion selective while a water-repelling pore favors the preferential adsorption of large ions. It was shown that, surprisingly, ion selectivity may be understood even without an explicit consideration of the confining geometry of the microchannels [16]. The classical DFT method was also used to study ion selectivity of a calcium channel modeled as a charged cylindrical pore [18]. Using the primitive model for confined ionic mixtures, Busath et al. indciated that the micropore shows selective absorption of calcium ions over sodium ions even if they have the same radius [18]. Similar models were used by Vlachy et al. to investigate ionic properties in charged cylinders based on the Poisson-Boltzmann (PB) equation and the grand canonical Monte Carlo (GCMC) simulation [19,20]. Good agreements between these two methods were observed for micropores with a moderate surface charge density. Figueroa et al. [21] and Malijevsky [22] used the FMT to study the selective adsorption of uncharged particles by cylindrical pores. Both groups found that the theoretical predictions were quite close to the GCMC results.

The aforementioned applications of classical DFT were mostly concerned either with uncharged systems or with spherical ions of the same size but different valences. However, ion adsorption and selectivity in realistic micropores reflect the coupled effects of electrostatic correlations and ionic excluded volume. In this work, we consider a more general case by incorporating excluded volume and electrostatic interactions within a single theoretical framework. Similar to previous publications, microchannels are represented by charged cylindrical pores of infinite length and the ionic mixtures are described as charged hard spheres in a continuous dielectric medium(*e.g.* aqueous solutions of alkali salts). Approximately, systems considered in this work mimic sodium and potassium channels as studied in previous investigations [18,23,11]. By investigating ion adsorption and selectivity for two positive ionic species in cylindrical pores of different radii and surface electrical potentials, we hope that the classical DFT predictions would shed new light on the joint effects of ionic size and electrostatic correlations.

2. Method

In this section, we recapitulate the coarse-grained model and the main equations for calculating the ionic density profiles and the local electrical potential in a cylindrical pore. Similar models have been used before for studying ion selectivity in nanochannels [14–17].

Consider a cylindrical pore of diameter $D = 2R$ in contact with a bulk electrolyte solution that consists of two types of cations and one type of anions in a dielectric medium. For simplicity, all ionic species are represented by charged hard spheres, and a hard-wall potential is used to describe short-range ion-surface interactions. In addition, we assume that the pore length is infinite, corresponding to conditions where the entrance effects are negligible. Fig. 1 schematically illustrates the geometric constraints for a spherical ion of radius R_i in such a cylindrical pore.

Because of the cylindrical symmetry, the ionic density profiles depend only on the radial distance to the central axis of the micropore, r. Assuming that the dielectric constant is uniform throughout space, we can apply the Poisson equation to relate the mean electrostatic potential, $\psi(r)$, and the ionic density profiles inside the pore, $\rho_i(r)$,

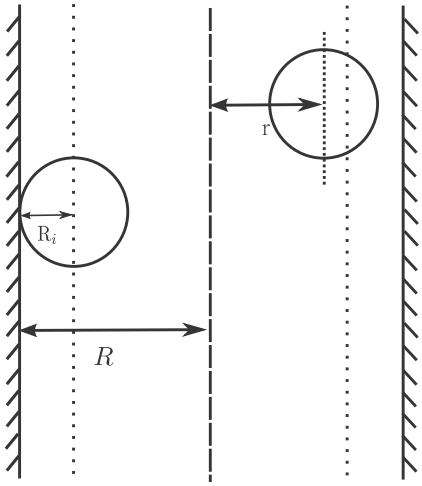

Fig. 1. Spherical ions in a cylindrical pore of radius R. Here r stands for the radial distance from the ion center to the central axis of the pore. The closest distance from the ion center to the pore surface is the same as the hard-sphere radius R_i.

$$\frac{1}{r}\frac{\partial}{\partial r}\left(r\frac{\partial\psi(r)}{\partial r}\right) = -\frac{e}{\epsilon_0\epsilon}\sum_i Z_i\rho_i(r), \tag{1}$$

where e represents the elementary charge, ϵ_0 is the absolute vacuum permittivity, ϵ is the solvent dielectric constant, Z_i and ρ_i are the valence and concentration of the ith ion species, respectively. Throughout this work, we fix the electrical potential at the surface of the cylindrical wall. Thus the Neumann boundary conditions for Eq. (1) are:

$$\psi'(0) = 0 \quad \psi(R) = \psi_0.$$

According to the Gauss theorem, charge neutrality is satisfied for the entire system, i.e., summation of the electrolyte charge and the surface charge is zero.

The ion distributions inside the pore can be predicted from the classical density functional theory (DFT) [24]

$$\rho_i(r) = \rho_i^0\exp\{-\beta Z_i e\psi(r) - \beta\Delta\mu_i^{ex}(r)\}, \tag{2}$$

where $\beta = 1/(k_BT)$, k_B is the Boltzmann constant, T is the absolute temperature, ρ_i^0 is the ion concentration in the bulk solution, and $\Delta\mu_i^{ex}(r) = \mu_i^{ex}(r) - \mu_b^{ex}$ is the difference between the local excess chemical potential of ion i and that in the bulk. Eq. (2) is in principle exact and implemented with the grand canonical ensemble [24]. If $\Delta\mu_i^{ex}(r) = 0$, Eqs. (1) and (2) reduce to the conventional Poisson-Boltzmann (PB) equation. Apparently, the PB equation neglects all interactions among ionic species except the mean electrostatic potential.

Within the coarse-grained model considered in this work, the excess chemical potential is composed of two parts, corresponding to contributions due to the hard-sphere (HS) repulsion and electrostatic correlation (EL),

$$\mu_i^{ex}(\boldsymbol{r}) = \mu_i^{HS}(\boldsymbol{r}) + \mu_i^{EL}(\boldsymbol{r}). \tag{3}$$

An accurate expression for the HS excess chemical potential can be obtained from the modified fundamental measure theory [25,26],

$$\beta\mu_i^{HS}(\boldsymbol{r}) = \sum_\alpha \int d\boldsymbol{r}'\varphi_\alpha(\boldsymbol{r}')\omega_i^\alpha(\boldsymbol{r}-\boldsymbol{r}'). \tag{4}$$

where the summation is taken over six local coefficients, $\varphi_\alpha(\boldsymbol{r})$, affiliated with corresponding weight functions ω_i^α introduced in the original FMT [10]. In Appendix A, we reproduce explicit expressions for the HS chemical potential in the cylindrical geometry.

We approximate the excess chemical potential due to the electrostatic correlation with that from a quadratic expansion of the excess Helmholtz energy with respect to the local density inhomogeneity [24]

$$\beta\mu_i^{EL}(\boldsymbol{r}) = \beta\mu_i^{EL}(\rho_i^0) - \sum_j \int \Delta\rho_j(\boldsymbol{r}')c_{ij}^{EL}(|\boldsymbol{r}-\boldsymbol{r}'|)d\boldsymbol{r}' \tag{5}$$

where $\Delta\rho_j(\boldsymbol{r}) = \rho_j(\boldsymbol{r}) - \rho_j^0$, $c_{ij}^{EL}(r)$ is the direct correlation function (DCF) due to electrostatic interactions, and the summation is taken over all ionic species. An analytic expression of DCF is available from the mean-spherical approximation (MSA) for bulk electrolytes[27,28].

To get the numerical results, we take integrations over the cylindrical pore on both sides of Eq. (1):

$$r\frac{\partial\psi(r)}{\partial r}\bigg|_r = -\frac{e_c}{\epsilon_0\epsilon}\sum_i Z_i\int_0^r s\rho_i(s)ds. \tag{6}$$

Eq. (6) can be further reduced to:

$$\frac{\partial\psi(r)}{\partial r} = \frac{A(r)}{r}, \tag{7}$$

in which $A(r) = -\frac{e_c}{\epsilon_0\epsilon}\sum_i Z_i\int_0^r s\rho_i(s)ds$. After a second integration on both side of Eq. (7), we have

$$\begin{aligned}\psi(r) &= \psi(0) + \int_0^r \frac{A(t)}{t}dt = \psi(0) + A(r)\ln r - \int_0^r A'(t)\ln t dt \\ &= \psi(0) - \frac{e_c}{\epsilon_0\epsilon}\sum_i Z_i\int_0^r s\rho_i(s)\ln r ds + \frac{e_c}{\epsilon_0\epsilon}\sum_i Z_i\int_0^r t\rho_i(t)\ln t dt \\ &= \psi(0) + \frac{e_c}{\epsilon_0\epsilon}\sum_i Z_i\int_0^r t\rho_i(t)\ln\frac{t}{r}dt.\end{aligned} \tag{8}$$

The concentration $\rho_i(r)$ can be obtained from Eq. (2) with the explicit formulas given in Appendix A. Eqs. (2) and (8) allow us to solve for both ionic concentrations and the electrostatic potential self-consistently. Specially, the Picard iteration is implemented to get the numerical results. The iteration is considered converged when the L2 -norm of $\Delta\hat{\rho}^i$ is smaller than 10^{-6} for all ion species, in which $\Delta\hat{\rho}^i = \hat{\rho}^i - \hat{\rho}^{i-1}$ and $\hat{\rho}^i$ is the reduced concentration values in the ith iteration.

3. Results and discussion

3.1. Validation of the DFT calculations

The free-energy functional used in our DFT calculations have been validated before with simulation data for ion distributions in slit pores or near planar/spherical surfaces [29]. However, much less has been studied for applications of the classical DFT to cylindrical systems, which is numerically more demanding. To validate the numerical procedure established in this work, we first consider a cylindrical pore containing a binary mixture of hard spheres with equal packing fractions but different radii, $R_1 = \sigma/2$ and $R_2 = \sigma$. The total packaging fraction of the system in the bulk is $\eta = 4\pi(\rho_1^0R_1^3 + \rho_2^0R_2^3)/3 = 0.4$. Because the diameter of large particles is twice that of the smaller ones, we have different reduced number densities for these particles in the bulk, $\rho_1^0\sigma^3 = 0.382$ and $\rho_2^0\sigma^3 = 0.0477$. Similar calculations had been reported before by Malijevsky but using the original fundamental measure theory (FMT) [22].

Fig. 2 shows the density profiles predicted by MFMT in comparison with GCMC simulations [22]. It is clear that the theoretical and simulation results are close to each other, affirming not only the accuracy of the classical DFT method but the correctness of our numerical procedure for implementation of MFMT in cylindrical coordinates. As expected, particle stratification inside the pore is noticeable with a rapid increase of the particle density near the cylindrical surface. At the center of the cylindrical pore, the reduced particle densities are close to their bulk values, 0.382 and 0.0477, respectively.

We have also calibrated the numerical procedure for charged systems. Fig. 3 shows the density profiles for an asymmetric electrolyte in a cylindrical pore with a positive surface charge. In this case, cations and anions have the same diameter σ but different valences, $Z_+ = 2$ and $Z_- = -1$. For comparison with simulation data, we fixed the surface

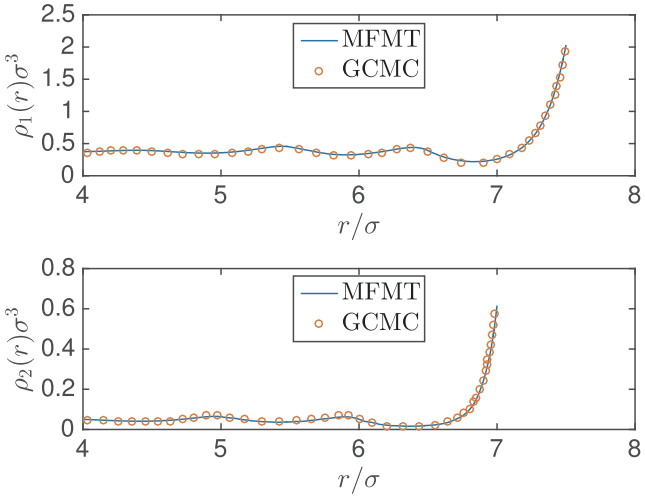

Fig. 2. The reduced densities of large and small particles inside a cylindrical pore containing a binary mixture of hard spheres of radii $R_1 = \sigma/2$ (upper panel) and $R_2 = 2R_1$ (lower panel), in which r is the radial distance from the central axis of the cylinder. The total packing fraction is $\eta = 0.4$, equally divided into those for small and large spheres, $\eta_1 = \eta_2 = 0.2$. The lines are from MFMT predictions and symbols are simulation results by Malijevsky [22].

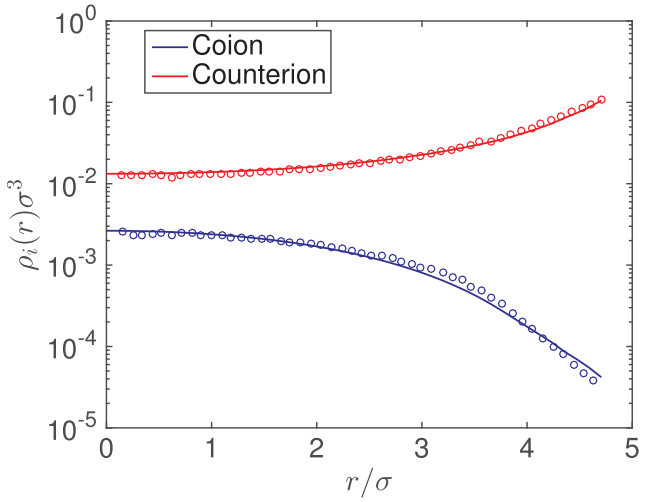

Fig. 3. Ionic density profiles for a 2:1 electrolyte solution in a cylindrical pore. Here cations and anions have the same diameter $\sigma_+ = \sigma_- = \sigma = 0.42$ nm, and the radius of the cylindrical pore is $R = 2.21$ nm. The electrolyte concentration in the bulk is 0.1099 M. The surface charge density of the cylindrical pore is $Q = 0.0712$ C/m^2. The solid lines are from the classical DFT predictions while the symbols are from GCMC simulation [20].

electrical potential in the DFT calculations and calculated the surface charge density of the cylindrical pore according to the neutrality condition for the entire system:

$$Q = -\frac{e}{R}\sum_i Z_i\int_0^R \rho_i(r)rdr. \tag{9}$$

Fig. 3 shows that the DFT predictions agree well with the GCMC data, furthering validating our computer program for predicting ionic distributions.

Although only two systems are considered in the above comparison, it is clear that our numerical procedure is accurate and that the classical DFT is able to reproduce simulation results reasonably well. Recently, Yu and coworkers reported more extensive calibration of the same version of the classical DFT with simulation results for cylindrical systems [30]. In the next subsection, we thus focus on ion selectivity in

charged cylindrical pores by using only the classical DFT calculations.

3.2. Local ionic densities and electrical potential in cylindrical pores

For studying ion selectivity by cylindrical pores of different radii and surface charge densities, we consider mixed electrolyte solutions containing two types of cations at equal concentration but only one type of anions. Approximately, these systems represent Na^+, K^+, and Cl^- ions dissolved in an aqueous solution ($\epsilon = 78$ for the background dielectric constant). Following a previous study [23], we assume that the diameters of these ions are $\sigma_{Na^+} = 1.94$ Å, $\sigma_{K^+} = 2.66$ Å, and $\sigma_{Cl^-} = 3.62$ Å. Two bulk concentrations are chosen for the positive ions in the reservoir. The total molar concentration for the dilute electrolyte solution is $C = 0.05$ M, which is close to that at the physiological condition [14,15]; and an electrolyte of higher total concentration, $C = 0.5$ M, is used as a reference. According to the neutrality condition in the reservoir, the Cl^- concentration is 0.1 M for the low concentration electrolyte and 1 M for the reference. Throughout this work, the cylindrical pore is assumed to have an infinite length and a uniform charge density. The condition of charge neutrality is aways satisfied for the whole system.

We consider first ion distributions in cylindrical pores of different radii under a fixed surface electrical potential. Fig. 4 presents the density profiles in a narrow pore that may accommodate at most a single layer of ions. At the low ion concentration ($C = 0.05$ M), the classical DFT predicts that the ionic density profile for each species is nearly constant along the radial direction. Although a weakly charged pore enriches small cations (Na^+) in terms of the total number of particles inside the pore, the local concentration of big cations (K^+) exceeds that for small cations at positions where both ions are accessible. The elevated concentration inside the pore means that K^+ ions are more strongly adsorbed than Na^+ ions, even though the total number of particles inside the pore is smaller due to its larger excluded volume. The size effect on ion partitioning remains the same as the absolute value of the surface charge density increases [31,32]. In the latter case, the contact density for each counterion is significantly higher than that in the center.

The assumption of uniform ion densities inside the pore was adopted in a previous work [16] for investigating the size selectivity of cylindrical pores. The same assumption was also used by Goulding et al. to study size selectivity by neutral micropores [14,15]. It is worth noting that the uniform density assumption is valid only for ions in a weakly charged pore at relatively low bulk electrolyte concentrations (e.g., near physiological conditions). It breaks down when the surface charge density is sufficiently high or, as shown in Fig. 4(b), when the micropore coexists with a bulk electrolyte at high concentrations. In the latter case, we see a monotonic increase of the local densities for both positive ions while the local density for the negative ions is still near uniform. Because the surface potential is the same for the two cases shown in Fig. 4, we may attribute the enhanced contact density at high concentration to the ionic excluded volume effects.

We find that the counterion concentration inside the pore is larger than that for coions when the electrolyte concentration in the bulk is low (Fig. 4a), whereas an opposite trend is observed at high bulk concentration (Fig. 4b). In the former case, a small local concentration of coions is intuitive because the electrostatic interaction plays a leading role; counterions accumulated inside the cylindrical pore depresses the local coion density. In the latter case, the increased counterion concentration leads to stronger screening effects and thus a reduced electric field caused by the surface charge and ionic interactions. Because of the reduced electric field and stronger excluded-volume effects, the coion concentration becomes higher than that of individual counterion species (but still lower than 1 M, the total counterion concentration in the bulk).

Fig. 5 presents the density profiles of the ionic species in a larger cylindrical pore, $R = 10$ Å. Here the ion concentrations in the bulk are fixed at $C^0_{Na^+} = C^0_{K^+} = 0.05$ M and $C^0_{Cl^-} = 0.1$ M. In subfigure (a), the surface electrical potential of the cylindrical pore is the same as that in Fig. 4(a), i.e., $\psi_0 = -0.01$ V; in subfigure (b), all particles are uncharged and the surface potential is set to zero. Different from near uniform distributions of cations and anions in a narrow pore, we see a gradual decline of the local coion concentration near the weakly charged surface, concomitant to a smooth increase of counterion concentrations. The inhomogeneous distributions of ionic species resemble those in a planar electric double layer (EDL). Similar to that in a narrow pore, the concentration of K^+ ions in the larger pore is uniformly higher than that for Na^+ ions. The contact value of Na^+ concentration exceeds that for K^+ because the former is closer to the surface (thus experiences a stronger electrostatic attraction).

Fig. 5 (b) compares the ionic density profiles discussed above with those corresponding to a hard-sphere system, i.e., a binary mixture of Na^+ and K^+ ions at the same bulk densities but without electrostatic interactions (and the Cl^- concentration is zero). Similar to the ionic system, we see a gradual increase of the local densities corresponding to Na^+ and K^+ ions near the surface. While the local concentration of K^+ particles is larger than that of Na^+ particles as in the charged case, such difference disappears quickly away from the surface (viz., when the radial distance is smaller than 5 Å). Without electrostatic interactions, the local densities of small and large particles at the pore center are virtually indistinguishable from their bulk values.

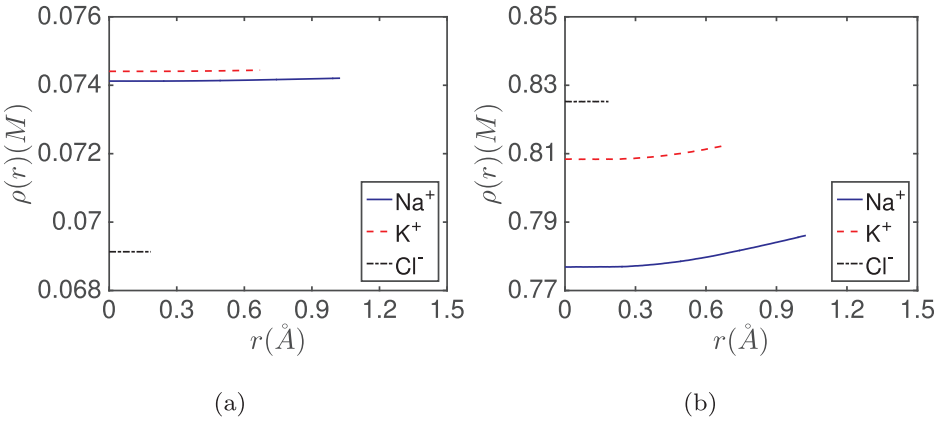

Fig. 4. Local ion densities in a cylindrical pore with a negative electrical potential at the surface, $\psi_0 = -0.01$ V. Here the cation concentrations in the bulk are (a) $C^0_{Na^+} = C^0_{K^+} = 0.05$ M and (b) $C^0_{Na^+} = C^0_{K^+} = 0.5$ M, respectively. The pore radius is 2 Å, and the ion diameters are 1.94 Å, 2.66 Å, 3.62 Å for Na^+, K^+ and Cl^-, respectively.

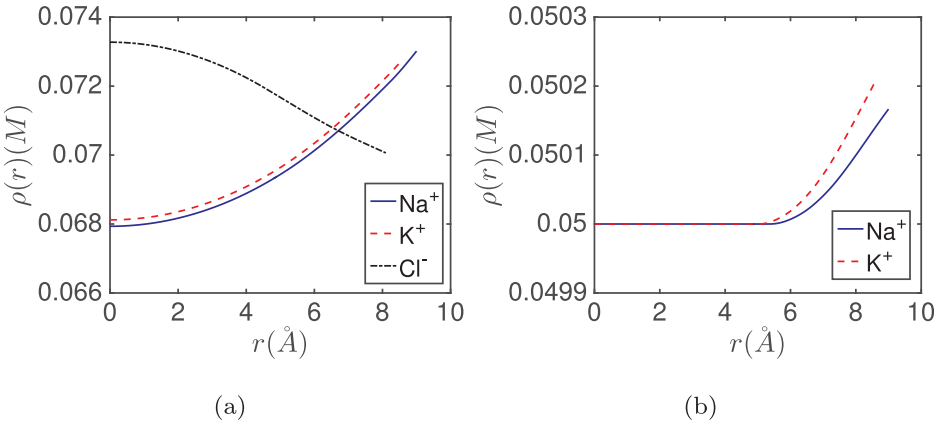

Fig. 5. (a) Ionic density profiles in a cylindrical pore of radius $R = 10$ Å. Here the cation concentrations in the bulk are $C^0_{Na^+} = C^0_{K^+} = 0.05$ M, and the surface electrical potential is $\psi_0 = -0.01$ V. (b) The same as (a) but for a uncharged system, i.e., a system that consists of neutral hard spheres with the number densities and the particle diameters the same as those for K^+ and Na^+ ions.

3.3. Ion partitioning and selectivity by nanopores of different electrical potentials and radii

To study the partitioning coefficients of ionic species between a cylindrical pore and the bulk solution, we define the mean density of each ionic species in terms of its accessible volume inside the cylindrical pore:

$$\overline{\rho}_\alpha = \frac{2}{(R-\sigma_\alpha/2)^2}\int_0^{R-\sigma_\alpha/2}\rho_\alpha(r)rdr. \tag{10}$$

The pore to bulk partitioning coefficient is given by

$$\zeta_\alpha = \overline{\rho}_\alpha/\rho^0_\alpha \tag{11}$$

where ρ^0_α is the bulk concentration for species α. It should be noted that the accessible volume, which is used here to define the average ion density (Eq. (10)), is different for ions of different sizes.

Fig. 6 presents the partitioning coefficients for the three ionic species in a cylindrical pore of radius 2 Å over a range of surface electrical potentials. Here the total electrolyte concentration in the bulk is fixed at 0.1 M. As expected, the partitioning coefficients for both cations fall monotonically as the absolute value of the surface potential is reduced, while an opposite trend is observed for anions. At zero electrical potential, the partitioning coefficients for all ion species are around unity, meaning that the average concentrations inside the pore are nearly the same as the bulk concentrations. When the surface potential is below −0.1 V, however, the partitioning coefficients for cations are greater than 50, while the value for anions nearly vanishes. In this case, the cylindrical pore is crowded with Na^+ and K^+, virtually no Cl^- ions can be found in the pore. Surprisingly, the classical DFT predicts that the difference between the partitioning coefficients of the two positive ions is negligible at all surface potentials (Fig. 6(a)). The value for K^+ is only slightly higher that for Na^+, indicating that the preferential adsorption of K^+ by the cylindrical pore is hardly noticeable when both electrostatic correlation and hard sphere repulsion are incorporated into the traditional DFT.

For most practical applications, the quantity of central interest is ion selectivity, which is defined as $\zeta = \zeta_{Na^+}/\zeta_{K^+}$ for the two cations considered in this work. Apparently, ion selectivity is different if the average density inside the pore is defined in terms of the total geometric volume. Fig. 7(a)–(d) illustrates the effect of surface electrical potential ψ_0 on the selectivity of Na^+ over K^+ by cylindrical pores of different radii. As shown in Fig. 7(a), the selectivity of Na^+ over K^+ is always smaller than 1 when the pore radius is 2 Å, meaning more favorable adsorption of K^+ ions. The preferential adsorption of larger cations is consistent with the density profiles shown in Fig. 4. The selectivity is appreciably enhanced at a higher electrolyte concentration in the bulk because of the increased excluded volume effects. Surprisingly, the pore becomes more selective to K^+ ions as the absolute value of the surface potential increases, even though that the contact energy for Na^+ ions is appreciably larger. The non-intuitive result may be attributed to near uniform distributions of ionic species in a narrow pore.

When the pore radius is 3 Å, the selectivity of the cylindrical pore is still below 1, indicating that the pore remains favorable for the adsorption of K^+ ions. At the low bulk concentration, an increase of the

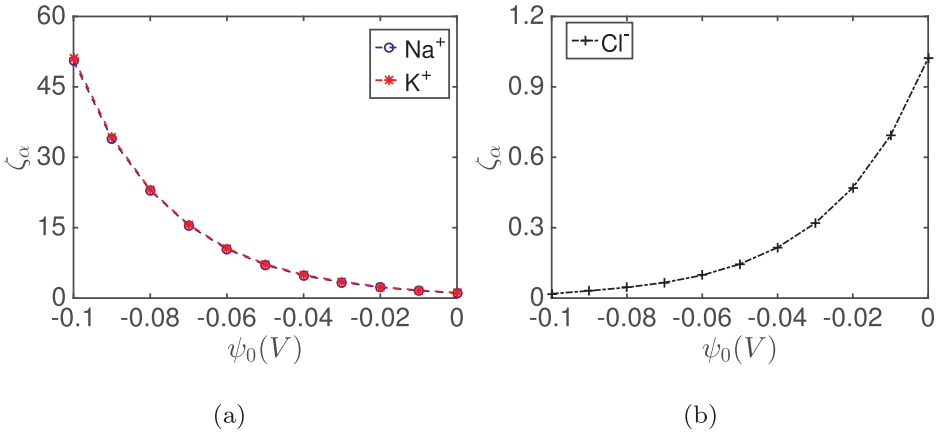

Fig. 6. Pore to bulk partitioning coefficients, ζ_α, for three types of ions, Na^+, K^+ and Cl^-, versus the surface electrical potential, ψ_0, of a cylindrical pore. Here the pore radius is $R = 2$ Å, and the ion concentrations in the bulk are 0.05 M, 0.05 M and 0.1 M, respectively, for Na^+, K^+ and Cl^- ions.

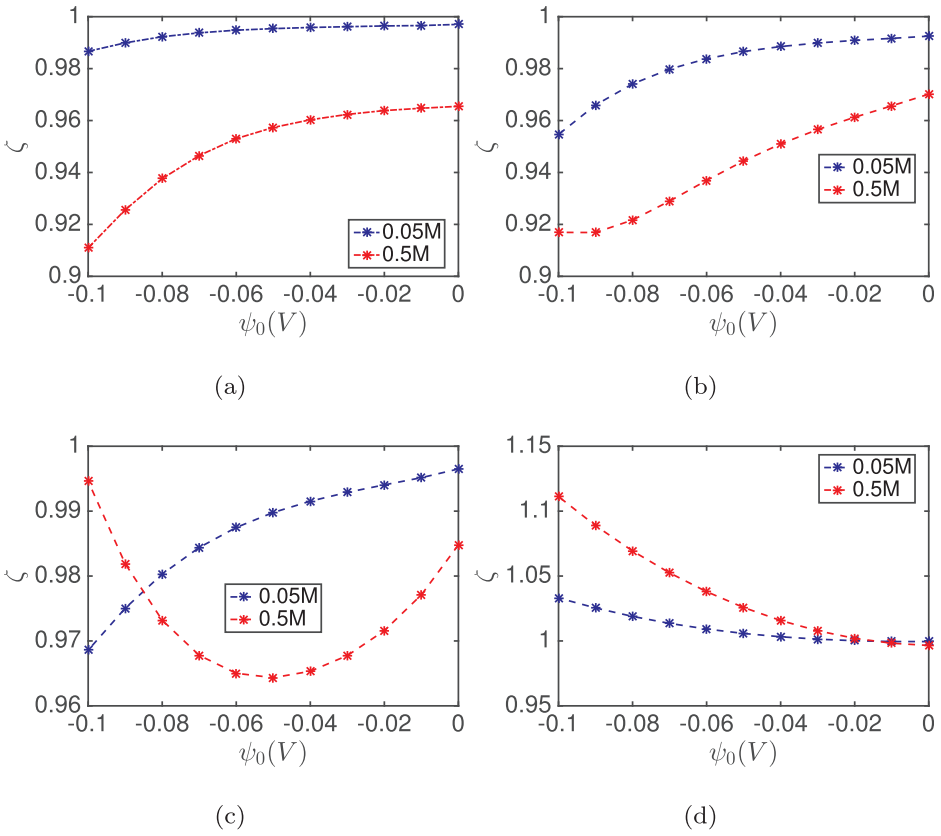

Fig. 7. The selectivity of Na^+ over K^+ for a cylindrical pore of radius: (a) $R = 2$ Å, (b) $R = 3$ Å, (c) $R = 4$ Å and (d) $R = 10$ Å.

absolute value of the surface potential enhances ion selectivity. However, the trend is opposite at high bulk concentrations. In the latter case, the selectivity does not change monotonically with the surface electric potential; the minimum selectivity occurs at an intermediate value, suggesting a competition between surface attraction (in favor of Na^+ ions) and excluded volume effects (in favor of K^+ ions).

As the pore radius is increased to 4 Å, the variation of the selectivity ζ with the surface potential ψ_0 is similar to that for the pore radius of 3 Å. When the surface potential is below -0.1 V, the pore favors the adsorption of Na^+ ions at high bulk concentration and K^+ ions at low bulk concentration. In other words, we can change the ion selectivity of a cylindrical pore by adjusting the bulk electrolyte concentration. Again the concentration dependence of the ion selectivity reflects the competing contributions due to electrostatic and excluded volume interactions. At the high bulk concentration, Fig. 7(c) suggests that an optimal surface potential can be identified to enhance the selective adsorption of K^+ ions.

Fig. 7(d) shows the ion selectivity for a cylindrical pore of radius $R = 10$ Å. In this case, the selectivity is larger than one and falls monotonically as the surface potential increases, indicating that a large pore of negative surface charge is always small ion (Na^+) selective. The trends are opposite to those for a small pore (Fig. 7(a)) because the ionic distribution is near uniform in a small pore but a large pore allows for the full development of the electric double layer near the charged surface. It is interesting to observe that a small pore selects larger ions while a large pore selects small ions. In both cases, the selectivity is enhanced as the bulk concentration increases. The selection of different ions by small and large pores reflects the complex interplay among electrostatic correlations and excluded volume effects.

Fig. 8 shows the partitioning coefficients for Na^+ and K^+ in a neutral pore. The partitioning coefficient falls sharply as the pore radius increases and approaches unity when the radius is beyond about $R = 5$ Å. The reduction in partitioning coefficient as the pore size increases can be attributed to less confinement effect. For ions in a large neutral pore, the average concentration for each ionic species is nearly the same as its bulk value. It is noticed that the partitioning coefficient at high bulk concentration is larger than that at low concentration when the radius is small ($R = 5$ Å). However, opposite trends are observed when the pore radius is large because of the competition between electrostatic correlation (favors ions in the bulk) and excluded volume effects (favors ion adsorption).

Fig. 9 shows that the selectivity value is always smaller than 1 for neutral cylindrical pores, indicating that a neutral pore favors the selective adsorption of larger ions (K^+). As aforementioned in the discussion for Fig. 5(b), the ion distribution inside a neutral pore is mainly determined by the excluded volume effects. Similar to a system of neutral hard spheres, the local concentration of potassium ions is aways larger than that of sodium ions, explaining why the relative selectivity value is smaller than 1. The influence of the hard-sphere repulsion becomes more significant as the electrolyte concentration increases or as the pore radius falls. In both cases, we observe a higher relative selectivity.

Fig. 10 illustrates the selectivity of Na^+ over K^+ versus the radius of a cylindrical pore at two representative surface potentials, $\psi_0 = -0.01$ V and -0.1 V, respectively. It is noticed that the ζ values are close to one according to our model, which accounts only electrostatic and hard-sphere interaction in a dielectric medium. The low selectivity may also be attributed to the condition settings of the bulk ion concentrations and applied voltages. Nevertheless, the slight difference helps to shed light on the mysterious phenomena of ion selectivity in biological systems. In both subfigures, the selectivity value is below unity in small pores and larger than one when the radius is sufficiently large. The selectivity becomes more sensitive to the pore radius as the electrolyte concentration or the surface potential increases. As mentioned above, a charged cylindrical pore is large-ion selective when the pore radius is small and turns into small-ion selective as the radius increases. A large

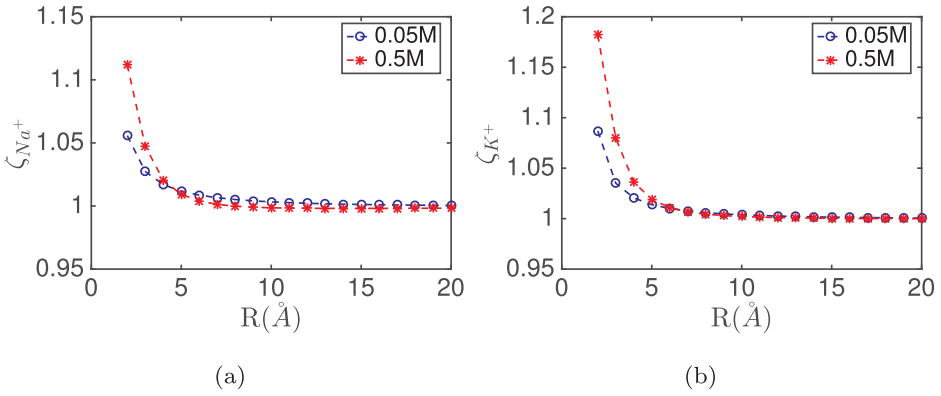

Fig. 8. The partition coefficients, ζ_α, versus the cylindrical radius R for (a) Na^+ and (b) K^+ when the surface potential is zero.

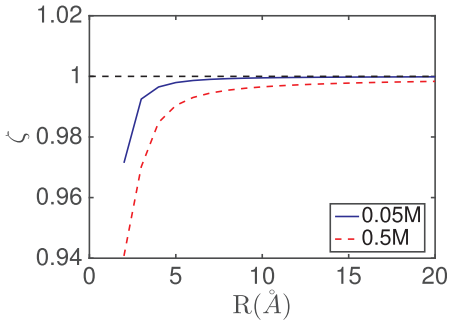

Fig. 9. The selectivity of Na^+ over K^+ when the surface electrical potential is zero.

cylindrical pore becomes more favorable for the adsorption of smaller counterions when the absolute value of the surface potential increases. The enhanced selectivity can be attributed to the rise in the difference between the surface energies of small and large ions. In this case, one may intuitively assert that the smaller ions neutralize the surface charge more efficiently than the bigger ions. For small cylinders, however, the excluded-volume effects play a leading role, favoring adsorption of more potassium ions in the pore.

4. Conclusions

Ion selectivity in cylindrical pores has been investigated by using the primitive model of aqueous electrolytes and the classical density functional theory (DFT). Whereas the coarse-grained model lacks chemical details, it accounts for electrostatic correlations and ionic excluded volume effects important for ion partitioning between a bulk solution and small pores. In comparison with molecular simulations, the ionic excluded volume effect can be accurately described by the modified fundamental measure theory and the mean-spherical approximation (MSA) provides an adequate description of the electrostatic correlations.

Following previous investigations [23], we adopt a mixed electrolyte solution containing an equal amount of potassium and sodium ions as the model system. While earlier studies of ion selectivity for similar systems were focused on hard-sphere repulsion or ions with the same diameter, this work provides a more comprehensive theoretical analysis by considering cylindrical pores of different surface charge densities and diameters. We find that ion distribution in a narrow cylindrical pore is nearly uniform regardless the bulk concentration or the surface potential. The electric double layer is fully developed only when the pore size is sufficiently large to accommodate multiple layers of ionic species. Whereas small counterions always have a more favorable contact energy, the local density of large counterions may surpass that of small counterions due to excluded volume effects. When the surface potential is zero, a cylindrical pore is always large-ion selective, and the selectivity is enhanced as the ion concentration in the bulk increases. However, the selectivity of charged cylinders is much more complicated. In systems with a small pore radius, it is observed that the cylinder favors preferential adsorption of large ions over small ions. While in systems with a large pore radius, the trend can be opposite. In both cases, the selectivity is enhanced as the bulk concentration increases. The selection of different ions at small and large pores is resulted from complex interplay among electrostatic correlations and excluded volume effects.

As observed in this work, it seems that only small selectivity can be anticipated in this type of models for ion channels over a wide range of conditions. In biology, both strong selective and weak/non selective ion channels exit. Some important factors which may play important roles in selectivity are missed in the current coarse-grained model, e.g. the

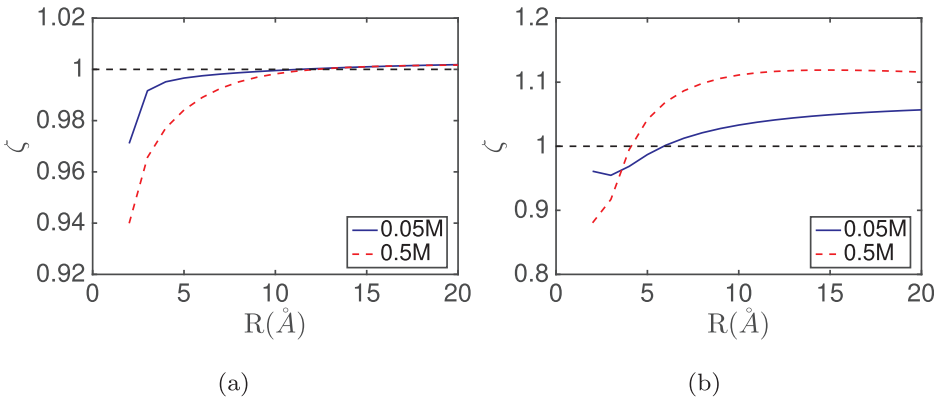

Fig. 10. The selectivity of Na^+ over K^+ when the surface potential is: (a) $\psi_0 = -0.01$ V and (b) $\psi_0 = -0.1$ V.

flexibility of the pore and surface heterogeneity, atomic polarizability, the variable dielectric and diffusion coefficients in the channel, exact electric correlation, dynamic (or time-dependent) properties of ion flow, and so on. Another important factor is the hydration effect, which may associates with desolvation processes during ion permeation in certain ion channels [33,34]. All these factors can be incorporated into future considerations to make the coarse-grained model more realistic. We hope that the results discussed in this work would provide useful insights for the development of novel porous materials to describe ion separation and energy storage and/or better understanding of ion selectivity in natural systems.

Acknowledgements

We thank Dr. Xian Kong for helpful discussions. Yu Qiao and Cheng Lian are grateful to the Chinese Scholarship Council for the visiting fellowship. Benzhuo Lu was sponsored by Science Challenge Project (No. TZ2016003), the National Key Research and Development Program of China (Grant No. 2016YFB0201304), and China NSF (NSFC 21573274, 11771435). Jianzhong Wu was supported by the Fluid Interface Reactions, Structures and Transport (FIRST) Center, an Energy Frontier Research Center funded by the U.S. Department of Energy, Office of Science, Office of Basic Energy Sciences.

Appendix A

In this appendix, we provide the explicit formulas of the excess chemical potential in the modified FMT in the special case of cylindrical cylinder. For the general case, the local HS excess chemical potential is given by

$$\beta\mu_i^{HS}(\boldsymbol{r}) = \sum_\alpha \beta\mu_{i,\alpha} = \sum_\alpha \int d\boldsymbol{r}'\varphi_\alpha(\boldsymbol{r}')\omega_i^\alpha(\boldsymbol{r}-\boldsymbol{r}').$$

in the summation, the coefficient $\varphi_\alpha(\boldsymbol{r}')$ is related to the definition of hard sphere Helmholtz free energy and ω_i^α is the weighted function originated from Rosenfeld's FMT [10], which is expressed as follows:

$$\omega_i^{(3)}(\boldsymbol{r}) = \theta(R_i-|\boldsymbol{r}|),$$
$$\boldsymbol{\omega}_i^{(V2)}(\boldsymbol{r}) = \nabla\theta(R_i-|\boldsymbol{r}|) = \frac{\boldsymbol{r}}{|\boldsymbol{r}|}\delta(R_i-|\boldsymbol{r}|),$$
$$\omega_i^{(2)}(\boldsymbol{r}) = |\nabla\theta(R_i-|\boldsymbol{r}|)| = \delta(R_i-|\boldsymbol{r}|).$$
$$\omega_i^{(1)}(\boldsymbol{r}) = \omega_i^{(2)}(\boldsymbol{r})/4\pi R_i,$$
$$\omega_i^{(0)}(\boldsymbol{r}) = \omega_i^{(2)}(\boldsymbol{r})/4\pi R_i^2,$$
$$\boldsymbol{\omega}_i^{(V1)}(\boldsymbol{r}) = \boldsymbol{\omega}_i^{(V2)}(\boldsymbol{r})/4\pi R_i.$$

In cylindrical cylinder, the local HS excess chemical potential can be reduced to

$$\beta\mu_{i,0}(r) = \frac{1}{4\pi}\int_0^{2\pi} d\varphi \int_{-1}^1 \phi_0(t_1)dt,$$
$$\beta\mu_{i,1}(r) = \frac{R_i}{4\pi}\int_0^{2\pi} d\varphi \int_{-1}^1 \phi_1(t_1)dt,$$
$$\beta\mu_{i,2}(r) = R_i^2\int_0^{2\pi} d\varphi \int_{-1}^1 \phi_2(t_1)dt,$$
$$\beta\mu_{i,3}(r) = \int_0^{2\pi} d\varphi \int_0^{\pi} \sin\theta d\theta \int_0^{R_i} \phi_3(t_2)t^2dt,$$
$$\beta\mu_i^{V1}(r) = \frac{1}{4\pi}\int_0^{2\pi} \int_{-1}^1 \phi_{V1}(t_1)\frac{t_1^2-s(s+R_it)}{t_1}dtd\varphi,$$
$$\beta\mu_i^{V2}(r) = R_i\int_0^{2\pi} \int_{-1}^1 \phi_{V2}(t_1)\frac{t_1^2-s(s+R_it)}{t_1}dtd\varphi.$$

in which

$$t_1^2 = s^2 + 2R_ist + R_i^2-R_i^2(1-t^2)\cos^2\varphi,$$
$$t_2^2 = s^2 + 2st\cos\theta + t^2-t^2\sin^2\theta\cos^2\varphi,$$
$$\phi_0 = -\ln(1-n_3),$$
$$\phi_1 = \frac{n_2}{1-n_3},$$
$$\phi_2 = \frac{n_1}{1-n_3} + \frac{n_3+(1-n_3)^2\ln(1-n_3)}{12\pi n_3^2(1-n_3)^2}(n_2^2-\vec{n}_{V2}^2),$$
$$\phi_3 = \frac{n_0}{1-n_3} + \frac{n_1n_2-\boldsymbol{n}_{V1}\cdot\boldsymbol{n}_{V2}}{(1-n_3)^2}-\frac{n_2^3-3n_2\boldsymbol{n}_{V2}^2}{36\pi}\left(\frac{2-5n_3+n_3^2}{(1-n_3)^3n_3^2} + \frac{2\ln(1-n_3)}{n_3^3}\right),$$
$$\boldsymbol{\phi}_{V1} = -\frac{\boldsymbol{n}_{V2}}{1-n_3},$$
$$\boldsymbol{\phi}_{V2} = -\frac{\boldsymbol{n}_{V1}}{1-n_3}-\frac{n_3+(1-n_3)^2\ln(1-n_3)}{6\pi n_3^2(1-n_3)^2}n_2\vec{n}_{V2},$$
$$\phi_{V1}(s) = |\boldsymbol{\phi}_{V1}(\boldsymbol{r})|,\ \phi_{V2}(s) = |\boldsymbol{\phi}_{V2}(\boldsymbol{r})|,$$
$$n_\alpha(\boldsymbol{r}) = \sum_i \int \rho_i(\boldsymbol{r}')\omega_i^{(\alpha)}(\boldsymbol{r}-\boldsymbol{r}')d\boldsymbol{r}',$$

and s is the radial distance to the center of the cylinder at the given point $\boldsymbol{r}$.

References

[1] I. Vlassiouk, S. Smirov, Z. Siwy, Ionic selectivity of single nanochannels, Nano Lett. 8 (2008) 1978–1985.
[2] T. Dudev, C. Lim, Competition among metal ions for protein binding sites: determinants of metal ion selectivity in proteins, Chem. Rev. 114 (2013) 538–556.
[3] B. Hille, Ion Channels of Excitable Membranes, third ed., Sinauer Asc., 2001.
[4] C. Lian, A. Gallegos, H. Liu, J. Wu, Non-scaling behavior of electroosmotic flow in voltage-gated nanopores, Phys. Chem. Chem. Phys. 19 (2017) 450–457.

[5] B. Tu, S. Bai, B. Lu, Q. Fang, Conic shapes have higher sensitivity than cylindrical ones in nanopore DNA sequencing, Sci. Rep. 8 (2018) 9097.
[6] B. Eisenberg, Crowded charges in ion channels, Advances in Chemical Physics, John Wiley & Sons, Inc., 2011, pp. 77–223.
[7] M.B. Ulmschneider, C. Bagnéris, E.C. McCusker, P.G. DeCaen, M. Delling, D.E. Clapham, J.P. Ulmschneider, B.A. Wallace, Molecular dynamics of ion transport through the open conformation of a bacterial voltage-gated sodium channel, Proc. Natl. Acad. Sci. USA 110 (2013) 6364–6369.
[8] D. Boda, M. Valiskó, B. Eisenberg, W. Nonner, D. Henderson, D. Gillespie, Combined effect of pore radius and protein dielectric coefficient on the selectivity of a calcium channel, Phys. Rev. Lett 98 (2007) 168102.
[9] D. Gillespie, Energetics of divalent selectivity in a calcium channel: the ryanodine receptor case study, Biophys. J. 94 (2008) 1169–1184.
[10] Y. Rosenfeld, Free-energy model for the inhomogeneous hard-sphere fluid mixture and density-functional theory of freezing, Phys. Rev. Lett. 63 (1989) 980–983.
[11] D. Gillespie, L. Xu, Y. Wang, G. Meissner, (De)constructing the ryanodine receptor: modeling ion permeation and selectivity of the calcium release channel, J. Phys. Chem. B 109 (2005) 15598–15610.
[12] J. Jiang, D. Cao, D. Jiang, J. Wu, Time-dependent density functional theory for ion diffusion in electrochemical systems, J. Phys.: Condens. Matter 26 (2014) 284102.
[13] Y. Qiao, X. Liu, M. Chen, B. Lu, A local approximation of fundamental measure theory incorporated into three dimensional Poisson-Nernst-Planck equations to account for hard sphere repulsion among ions, J. Stat. Phys. 163 (2016) 156–174.
[14] D. Goulding, J. Hansen, S. Melchionna, Size selectivity of narrow pores, Phys. Rev. Lett. 85 (2000) 1132–1135.
[15] D. Goulding, S. Melchionna, J. Hansen, Entropic selectivity of microporous materials, Phys. Chem. Chem. Phys. 3 (2001) 1644–1654.
[16] R. Roth, D. Gillespie, Physics of size selectivity, Phys. Rev. Lett. 95 (2005) 247801.
[17] Q. Shao, J. Zhou, L. Lu, X. Lu, Y. Zhu, S. Jiang, Anomalous hydration shell order of na^+ and k^+ inside carbon nanotubes, Nano Lett. 9 (2009) 989–994.
[18] D. Busath, D. Henderson, S. Sokolowski, Density functional theory for an electrolyte in a cylinder: the selectivity of a calcium channel, J. Phys.: Condens. Matter 16 (2004) S2193.
[19] V. Vlachy, A. Haymet, Electrolytes in charged micropores, J. Am. Chem. Soc. 111 (1989) 477–481.
[20] B. Jamnik, V. Vlachy, Monte Carlo and Poisson-Boltzmann study of electrolyte exclusion from charged cylindrical micropores, J. Am. Chem. Soc. 115 (1993) 660–666.
[21] S. Figueroa-Gerstenmaier, F. Blas, J. Avalos, L. Vega, Application of the fundamental measure density functional theory to the adsorption in cylindrical pores, J. Chem. Phys. 118 (2003) 830–842.
[22] A. Malijevsky, Fundamental measure theory in cylindrical geometry, J. Chem. Phys. 126 (2007) 134710.
[23] D. Boda, D. Henderson, D. Busath, Monte Carlo study of the effect of ion and channel size on the selectivity of a model calcium channel, J. Phys. Chem. B 105 (2001) 11574–11577.
[24] J. Wu, T. Jiang, D.-E. Jiang, Z. Jin, D. Henderson, A classical density functional theory for interfacial layering of ionic liquids, Soft Matter 7 (2011) 11222–11231.
[25] Y. Yu, J. Wu, Structures of hard-sphere fluids from a modified fundamental measure theory, J. Chem. Phys. 117 (2002) 10156–10164.
[26] R. Roth, R. Evans, A. Lang, G. Kahl, Fundamental measure theory for hard-sphere mixtures revisited: the White Bear version, J. Phys.: Condens. Matter 14 (2002) 12063–12078.
[27] K. Hiroike, Supplement to Blum's theory for asymmetric electrolytes, Mol. Phys. 33 (1977) 1195–1198.
[28] L. Blum, Mean spherical model for asymmetric electrolytes I: method of solution, Mol. Phys. 30 (1975) 1529–1535.
[29] D.H.J. Jiang, D. Cao, J. Wu, Revisiting density functionals for ionic distributions in electric double layers, J. Chem. Phys. 140 (2014) 044714.
[30] Y. Xin, Y. Zheng, Y. Yu, Density functional theory study on ion adsorption and electroosmotic flow in a membrane with charged cylindrical pores, Mol. Phys. 114 (2016) 12328–12336.
[31] M. Valiskó, D. Boda, D. Gillespie, Selective adsorption of ions with different diameter and valence at highly charged interfaces, J. Phys. Chem. C 111 (2007) 15575–15585.
[32] C.-H. Hou, P. Taboada-Serrano, S. Yiacoumi, C. Tsouris, Electrosorption selectivity of ions from mixtures of electrolytes inside nanopores, J. Chem. Phys. 129 (2008) 224703.
[33] X. Liu, B. Lu, Incorporating born solvation energy into the 3d poisson-nernst-planck model to study ion selectivity in KcsA K+ channels, Phys. Rev. E 96 (2017) 062416.
[34] W. Kopec, D.A. Kpfer, O.N. Vickery, A.S. Bondarenko, T.L.C. Jansen, B.L. de Groot, U. Zachariae, Direct knock-on of desolvated ions governs strict ion selectivity in K+ channels, Nat. Chem. 10 (2018) 813–820.